15 Bellentani S, Saccoccio G, Costa G *et al.* Drinking habits as cofactors of risk for alcohol induced liver damage. The Dionysos Study Group. *Gut* 1997; **41**: 845–50.
16 Kawamura Y, Arase Y, Ikeda K *et al.* Large-scale long-term follow-up study of Japanese patients with non-alcoholic fatty liver disease for the onset of hepatocellular carcinoma. *Am. J. Gastroenterol.* 2012; **107**: 253–61.
17 Kodama K, Tokushige K, Hashimoto E, Taniai M, Shiratori K. Hepatic and extrahepatic malignancies in cirrhosis caused by nonalcoholic steatohepatitis and alcoholic liver disease. *Alcohol. Clin. Exp. Res.* 2013; **37** (Suppl. 1): E247–52.
18 Sanyal AJ, Banas C, Sargeant C *et al.* Similarities and differences in outcomes of cirrhosis due to nonalcoholic steatohepatitis and hepatitis C. *Hepatology* 2006; **43**: 682–9.
19 Ascha MS, Hanouneh IA, Lopez R, Tamimi TA, Feldstein AF, Zein NN. The incidence and risk factors of hepatocellular carcinoma in patients with nonalcoholic steatohepatitis. *Hepatology* 2010; **51**: 1972–8.
20 Hashimoto E, Tokushige K. Hepatocellular carcinoma in non-alcoholic steatohepatitis: growing evidence of an epidemic? *Hepatol. Res.* 2012; **42**: 1–14.
21 Yasui K, Hashimoto E, Komorizono Y *et al.* Characteristics of patients with nonalcoholic steatohepatitis who develop hepatocellular carcinoma. *Clin. Gastroenterol. Hepatol.* 2011; **9**: 428–33.
22 Tokushige K, Hashimoto E, Yatsuji S *et al.* Prospective study of hepatocellular carcinoma in nonalcoholic steatohepatitis in comparison with hepatocellular carcinoma caused by chronic hepatitis C. *J. Gastroenterol.* 2010; **45**: 960–7.
23 Zen Y, Katayanagi K, Tsuneyama K, Harada K, Araki I, Nakanuma Y. Hepatocellular carcinoma arising in non-alcoholic steatohepatitis. *Pathol. Int.* 2001; **51**: 127–31.

HEPATOLOGY
Official Journal of the American Association for the Study of Liver Diseases
AASLD

Contrast-Enhanced Intraoperative Ultrasonography for Vascular Imaging of Hepatocellular Carcinoma: Clinical and Biological Significance

Kota Sato,[1] Shinji Tanaka,[1] Yusuke Mitsunori,[1] Kaoru Mogushi,[2] Mahmut Yasen,[1] Arihiro Aihara,[1] Daisuke Ban,[1] Takanori Ochiai,[1] Takumi Irie,[1] Atsushi Kudo,[1] Noriaki Nakamura,[1] Hiroshi Tanaka,[2] and Shigeki Arii[1]

Abnormal tumor vascularity is one of the typical features of hepatocellular carcinoma (HCC). In this study, the significance of contrast-enhanced intraoperative ultrasonography (CEIOUS) images of HCC vasculature was evaluated by clinicopathological and gene expression analyses. We enrolled 82 patients who underwent curative hepatic resection for HCC with CEIOUS. Clinicopathological and gene expression analyses were performed according to CEIOUS vasculature patterns. CEIOUS images of HCC vasculatures were classified as reticular HCC or thunderbolt HCC. Thunderbolt HCC was significantly correlated with higher alpha-fetoprotein levels, tumor size, histological differentiation, portal vein invasion, and tumor-node-metastasis stage, and these patients demonstrated a significantly poorer prognosis for both recurrence-free survival ($P = 0.0193$) and overall survival ($P = 0.0362$) compared with patients who had reticular HCC. Gene expression analysis revealed that a rereplication inhibitor geminin was significantly overexpressed in thunderbolt HCCs ($P = 0.00326$). *In vitro* knockdown of geminin gene reduced significantly the proliferation of human HCC cells. Immunohistochemical analysis confirmed overexpression of geminin protein in thunderbolt HCC ($P < 0.0001$). Multivariate analysis revealed geminin expression to be an independent factor in predicting poor survival in HCC patients ($P = 0.0170$). *Conclusion*: CEIOUS vascular patterns were distinctly identifiable by gene expression profiling associated with cellular proliferation of HCC and were significantly related to HCC progression and poor prognosis. These findings might be clinically useful as a determinant factor in the postoperative treatment of HCC. (HEPATOLOGY 2013;57:1436-1447)

Hepatocellular carcinoma (HCC) is the fifth most common malignancy and one of the most common causes of cancer-related death in the world.[1,2] Surgical resection is considered the primary curative therapy in the treatment of HCC.[3-5] During hepatic resection, intraoperative ultrasonography (IOUS) of the liver is used as an aid for surgical navigation. IOUS provides crucial diagnostic and staging information to the surgeon during the procedure.[6] Recently, contrast-enhanced ultrasonography techniques using microbubble agents have been developed.[7] Among these agents, Sonazoid (gaseous perflubutane; Daiichi-Sankyo, Tokyo, Japan) is a unique ultrasound contrast agent that is accumulated in Kupffer cells.[8-12] We reported recently that Kupffer imaging of Sonazoid with contrast-enhanced intraoperative ultrasonography (CEIOUS) is quite useful for detailed detection of tumors in real time during hepatic resection.[13]

Tumor angiogenesis is one of the critical features in determining overgrowth and metastatic potential.[14,15] In contrast to normal vessels, tumor vessels are tortuous, excessively branched, and short-circuited. In this manner, tumor vasculature is highly disorganized.[14-18] HCC is a tumor that is typically known to exhibit

Abbreviations: AFP, alpha-fetoprotein; CEIOUS, contrast-enhanced intraoperative ultrasonography; FC, fold change; HCC, hepatocellular carcinoma; IOUS, intraoperative ultrasonography; MFI, micro-flow imaging; PBS, phosphate-buffered saline; preRC, prereplication complex; siRNA, small interfering RNA; TNM, tumor-node-metastasis.

From the [1]Department of Hepato-Biliary-Pancreatic Surgery, Graduate School of Medicine; and the [2]Information Center for Medical Sciences, Tokyo Medical and Dental University, Tokyo, Japan.

Received April 16, 2012; accepted October 20, 2012.

Supported by a Grant-in-Aid for Scientific Research on Innovative Areas, Scientific Research (A) from the Ministry of Education, Culture, Sports, Science & Technology of Japan and a Health & Labour Sciences Research Grant from the Ministry of Health Labour & Welfare of Japan.

angiogenesis.[2,3,18-23] In particular, a dramatic alteration in arterial hypervascularity is observed in moderately and poorly differentiated HCC.[18,20,21] Such hypervascularity can be observed using angiography and contrast-enhanced computed tomography,[21,24,25] but it is quite difficult to analyze the detailed intratumoral vasculature in real time.

Recently, it has been reported that contrast-enhanced ultrasonography can be used to evaluate tumor vasculature similarly to what is seen with other contrast-enhanced radiological imaging techniques.[22,23,34] In the present study, the HCC vasculature was analyzed in detail by CEIOUS with Sonazoid to identify the specific patterns associated with clinicopathological features. Additionally, genome-wide gene expression was assessed via DNA microarray analysis, which offers a systematic approach to acquire comprehensive information regarding gene transcription profiles.[26] Such studies could lead not only to the identification of unique biomarkers but also to the development of a novel molecular-targeted therapy for HCC.[27-30] The present study demonstrates the evidence indicating the biological and clinical significance of CEIOUS microflow imaging (MFI).

Patients and Methods

Patients and Samples. We enrolled patients who underwent curative hepatic resection for HCC at the Tokyo Medical and Dental University Hospital between August 2007 and March 2010. From a total of 167 patients with HCC, 135 patients underwent CEIOUS of the main tumor during hepatic resection. Among them, 82 patients were technically eligible for MFI analysis. The other 53 patients were technically ineligible for MFI mainly because of pretreatment with sorafenib, radiofrequency ablation, and transcatheter arterial chemoembolization. The baseline characteristics of the enrolled patients are summarized in Table 1. Written informed consent was obtained from the patients, and the institutional review board approved the study. The preoperative evaluations have been described elsewhere.[31] Resected tissue containing no necrosis was divided into two specimens immediately after surgery: one was snap-frozen in liquid nitrogen and stored at −80°C for microarray analysis; the other was fixed in 10% formaldehyde solution and embedded in paraffin for histopathological analysis. According to *The General Rules for the Clinical and Pathological Study of Primary Liver Cancer*,[32] histopathological analysis was performed. To confirm the expression patterns detected by the microarrays, the median follow-up period was 784 days (interquartile range, 497-1,015).

Table 1. Patient Characteristics

Characteristic	Value
Age, years, mean ± SD (range)	70 ± 9.0 (34-84)
Sex, no., male:female	62:20
Viral infection, no., HBV:HCV:non-B/C	13:46:23
Background liver pathology, no.	
Normal	6
Chronic hepatitis or liver fibrosis	33
Liver cirrhosis	43
Child-Pugh classification, no., A:B	78:4
Albumin, mg/dL, mean ± SD	4.1 ± 0.4
Total bilirubin, mg/dL, mean ± SD	0.90 ± 0.40
PT%, mean ± SD	82.2 ± 8.0
AFP, ng/mL, mean ± SE	5,751 ± 4,832
PIVKA-II, mAU/mL, mean ± SE	7,355 ± 3,575
Tumor size, cm, mean ± SD	4.2 ± 3.4 (1-25)
Tumor number, no., solitary:multiple	49:33
TNM stage, I:II:III:IV	5:28:32:17

HBV, hepatitis B virus, HCV, hepatitis C virus; PIVKA-II, protein induced by vitamin K absence or antagonist II; PT%, prothrombin time.

Analysis of MFI via CEIOUS. The ultrasound system Xario-XG (Toshiba Medical) was used for all IOUS and CEIOUS procedures with a 7-MHz, T-shaped linear probe (PLT-705BTH; Toshiba Medical). CEIOUS was performed with pulse inversion harmonic imaging capability. The mechanical index was set at 0.15 in all CEIOUS procedures. The acoustic power was altered to keep the mechanical index at 0.15 because the depth of the focus point varied. During CEIOUS procedures, a real-time fundamental mode image was displayed simultaneously with a pulse inversion harmonic image side-by-side for reference. Thus, the target lesions were not missed even if they were difficult to recognize in the pulse inversion harmonic imaging. During the operation, the liver was mobilized off the diaphragm for improved sonographic visualization. IOUS was then performed in a systematic fashion in baseline fundamental mode scan to

Address reprint requests to: Shinji Tanaka, M.D., Ph.D., F.A.C.S., Department of Hepato-Biliary-Pancreatic Surgery, Graduate School of Medicine, Tokyo Medical and Dental University, 1-5-45 Yushima, Bunkyo-ku, Tokyo 113-8519, Japan. E-mail: shinji.msrg@tmd.ac.jp; fax: (81)-3-5803-0263.

View this article online at wileyonlinelibrary.com.

DOI 10.1002/hep.26122

Potential conflict of interest: Nothing to report.

Additional Supporting Information may be found in the online version of this article.

confirm the preoperative tumor staging. There was no lesion discovered in the preoperative staging found during IOUS. After IOUS, Sonazoid was injected at a dose of 0.5 mL/body in approximately 1 second through a catheter inserted in the antecubital vein, followed by a 10-mL normal saline flush. Following injection, a dynamic CEIOUS was performed with the focus depth beyond the main tumor. The main tumor was observed continuously for approximately 1 minute from the time of injection (vascular phase). The arterial phase was timed for 45 seconds after completion of the flash, after which the portal venous phase was timed from 45 to 70 seconds after injection. We performed MFI after observation of the portal venous phase. For MFI analysis, the combination of flash replenishment sequence and the maximum intensity holding sequence was expected to make it possible to visualize the tumor vasculature clearly with high special resolution and vascular continuity.[23] The accumulation time for each MFI sequence was 10-15 seconds, depending on the perfusion of the target tissue. As the standardized procedure, we applied three-time flashes on the main tumor and confirmed the MFI pattern based on the dominant image during CEIOUS. At approximately 10-15 minutes after injection, ultrasonic observation was resumed using pulse inversion harmonic imaging in the systematic liver (Kupffer phase). Hypoechoic lesions were searched for in hyperechoic surrounding liver with accumulated microbubbles. The focus point was set at the bottom of the liver. In the case of new lesions detected, we performed defect reperfusion imaging with an additional injection of Sonazoid (0.5 mL/body). The observation in the Kupffer phase was not repeated after the second injection because all focal liver lesions were theoretically examined by a thorough scan in the first Kupffer phase. We removed all lesions diagnosed as HCC by each modality under conditions that ensured safety. The IOUS and CEIOUS scans and image analysis were performed in consensus reading by surgeons with 8, 10, 20, and 40 years of experience in liver surgery.

DNA Microarray Analysis. For the gene expression analysis, at least three sections of the largest nodule were used from the largest cross-section of the main tumor. Total RNA was extracted from the HCC specimens with an RNeasy kit (Qiagen, Hilden, Germany). The integrity of the RNA obtained was assessed with an Agilent 2100 Bioanalyzer (Agilent Technologies, Palo Alto, CA). Among the HCC tumors limited to $\leq$4 cm in diameter to exclude the bias of tumor size, 27 samples (11 reticular HCC, 16 thunderbolt HCC) were available for analysis of gene expression. In the 27 samples, the mean size of the tumor was 2.9 $\pm$ 0.2 cm. Contaminating DNA was removed by digestion with RNase-free DNase (Qiagen), and with 2 μg of total RNA, complementary RNA was prepared with a one-cycle target labeling and control reagents kit (Affeymetrix, Santa Clara, CA). The hybridization and signal detection of the Human Genome U133 (HG-U133) Plus 2.0 arrays (Affymetrix) were performed in accordance with the manufacturer's instructions. A total of 37,743 microarray data sets were normalized by the robust multiarray average method (R2.4.1 statistical software together with the BioConductor package), essentially as described in our previous report.[31] The estimated gene expression levels were log 2 transformed, and the fold change (FC) values were calculated using ratios of genometric means of gene expression levels between two MFI patterns. A Wilcoxon rank sum test was performed to estimate the significance levels of the differences in gene expression between the two groups. For each statistical test, the obtained P values from the multiple hypothetical testing were adjusted by a false discovery rate, and probe sets with a false discovery rate <0.47 were considered for further analysis. Hierarchical clustering with the selected probe sets was performed using a plete linkage method. For visualization, the expression levels were standardized as z scores (mean = 0, variance = 1) for each probe set.

Cell Culture. The human HCC cell lines SK-Hep1, Hep3B, and PLC/PRF/5 were obtained from American Type Culture Collection (Manassas, VA). The other human HCC cell lines Huh1, Huh7, HLE, HLF, and HepG2 were obtained from the Human Science Research Resources Bank (Osaka, Japan). The culture media used were Roswell Park Memorial Institute 1640 medium (SK-Hep1, Hep3B, Huh7, and HepG2) and Dulbecco's modified Eagle medium (PLC/PRF/5, Huh1, HLE, and HLF) supplemented with 5% fetal bovine serum for the HLF cells or 10% fetal bovine serum for the remaining cell lines. All media were supplemented with 100 U/mL of penicillin and 100 μg/mL of streptomycin. All cell lines were cultivated in a humidified incubator at 37°C in 5 % carbon dioxide and were collected with 0.25% trypsin-0.03% ethylene diamine tetraacetic acid.

Western Blotting and Immunocytochemistry. Geminin protein expression in the cell lines was detected via western blotting analysis. The total protein was extracted from each cell line as described.[33] The protein levels of geminin and α-tubulin (control) were detected via standard western blot analysis by using 8-15% sodium dodecyl sulfate–polyacrylamide gel electrophoresis.

The blots were incubated overnight at 4°C with the primary antibody, anti-human geminin (1:200; Santa Cruz Biotechnology, Santa Cruz, CA; catalog #sc-13015), and then at room temperature for 1 hour with anti–α-tubulin (1:5,000; Sigma-Aldrich, St.Louis, MO; catalog #T9026). The appropriate secondary antibodies were added for 2 hours, and the protein expression was visualized with enhanced chemiluminescence by the ECL western blot testing detection system (GE Healthcare, Buckinghamshire, UK). The immunocytochemical analysis was performed with cultured cells on glass slides coated with saline. The cells were fixed in phosphate-buffered saline (PBS)-10% trichloroacetic acid for 15 minutes, permeabilized in PBS-0.2% Triton X-100 for 5 minutes, and then blocked in PBS-3% bovine serum albumin for the immunocytochemical detection of geminin. The primary antibody (Santa Cruz Biotechnology) was used at 1:50 dilution, and γ-tubulin antibody (Sigma-Aldrich; catalog #T6557) was used at 1:1,000. The secondary antibody for geminin was the Alexa Fluor 568 fragment of a donkey anti-rabbit immunoglobulin G (H+L) and antibody for γ-tubulin was the Alexa Fluor 488 fragment of a donkey anti-mouse immunoglobulin G (H+L) (Invitrogen, Carsbad, CA). The DNA was counterstained with 4',6-dia-midino-2-phenylindeole. Image acquisition was performed on a confocal microscope (Axio Observer.ZL, Carl Zeiss Microimaging GmbH, Germany).

Gene Silencing. The knockdown of geminin was performed by using small interfering RNA (siRNA) (Invitrogen; catalog #1299003) and negative control siRNA duplexes (Invitrogen; catalog #12935112). HLF, SK-Hep1, and Hep3B cells were seeded at a density of 1.0×10^5 cells into 6-well plates in 2,000 μL of culture medium with 5% fetal bovine serum for the HLF cells or 10% fetal bovine serum for Hep3B and SK-Hep1 (for western blot testing, cell proliferation analysis, cell cycle analysis). Thereafter, transfection with the siRNA was performed by using Lipofectamine 2000 (Invitrogen) according to the manufacturer's instructions. After transfection, the cells were incubated for 96 hours at 37°C in a 5% carbon dioxide atmosphere. At the 0-, 24-, 48-, 72-, and 96-hour time points after siRNA transfection, cells were detached from each plate. The number of viable cells was counted by an automatic cell counting machine (CYTORECON; GE Healthcare) according to the manufacturer's instructions. The number of nonviable cells was assessed using CYTORECON and trypan blue dye exclusion. These experiments were independently evaluated in triplicate for cell proliferation analysis. And fluorescence-activated cell sorting for cell cycle analysis was done on cells that were collected by trypsinization on each point after siRNA transfection cells, fixed with 70% ethanol overnight at 4°C. Cells were rehydrated in PBS and then resuspended in PBS containing 100 μg/mL RNase (Sigma) and 10 μg/mL propidium iodide. Cellular DNA content was analyzed with a FACSCaliber flow cytometer (Becton Dickinson Biosciences, San Joes, CA) using Cellquest software.

Immunohistochemical Analysis. Immunohistochemical analysis was performed on HCC tissue samples. The primary antibodies were used at the following concentrations diluted in PBS containing 1% bovine serum albumin: geminin (1:500; Santa Cruz Biotechnology), Ki67 (1:100; Abcam, Cambridge, UK; catalog #ab833), EpCAM (1:3,000; AbD Serotec, Oxford, UK; catalog #MCA1870G), CK19 (1:100; Dako, Glostrup, Denmark; catalog #M088801), and c-KIT (Ventana XT System; Ventana, Tucson, AZ; catalog 790-2951). The tissue sections were stained by an automated immunostainer (Ventana XT System) using heat-induced epitope retrieval and a standard DAB detection kit (Ventana). The immunostaining was evaluated quantitatively by counting at least 500 cells in three different random fields (magnification ×100) under a light microscope by three independent investigators (Sato, Tanaka, and Arii). The mean value was calculated for the final result of each case.

Statistical Analysis. Statistical comparisons of clinicopathological characteristics for significance were performed using a χ^2 test or Fisher's exact test with a single degree of freedom, and a Student t test was used to analyze the differences between continuous values. Overall survival and recurrence rates were determined by the Kaplan-Meier method, and for comparisons, log-rank tests were used. P values less then 0.05 were considered to have statistical significance. To investigate those factors that predicted overall survival, multivariate analyses were performed using Cox proportional hazard models and logistic regression models. All statistical analyses were performed using SPSS version 17.0 (SPSS, Chicago, IL).

Results

Classification of MFI Patterns and Postoperative Outcomes of Patients with HCC. A total of 82 patients who underwent CEIOUS examination during hepatic resection of HCC were analyzed. According to MFI data, tumor vasculatures were classified as two characteristic patterns: a thin, ramified pattern (reticular HCC) and a thick, linear pattern (thunderbolt HCC), although such a difference could not be

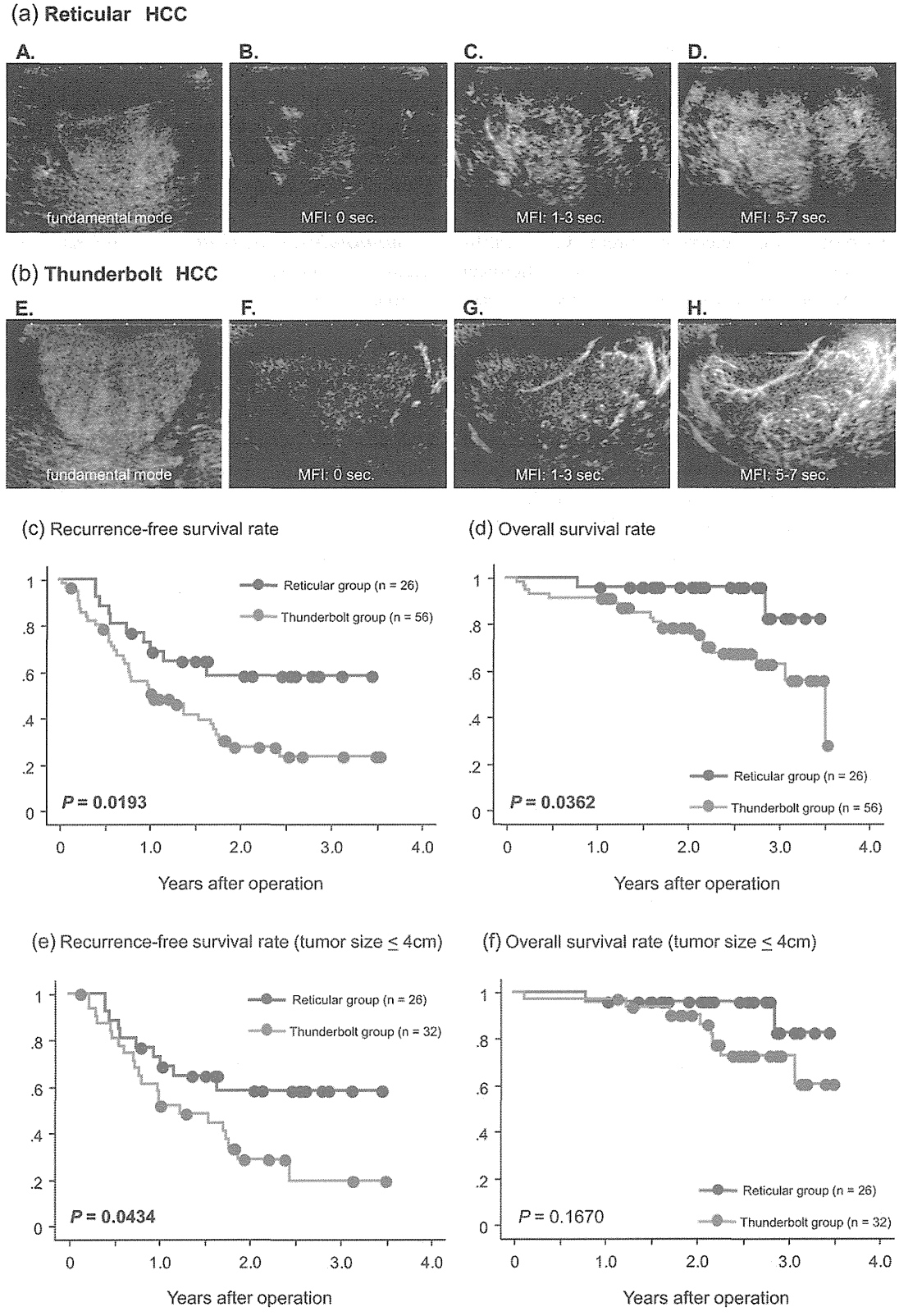

Fig. 1. Classification of CEIOUS MFI patterns with HCC. Using the MFI data, the HCC vasculatures were classified into two characteristic types; (a) reticular HCC and (b) thunderbolt HCC. While reticular HCC was gradually enhanced to the entire tumor with thin and ramified vessels (B-D), thunderbolt HCC was enhanced in a part of tumor with thick and linear vessels (F-H). The fundamental mode of ultrasonography is shown (A, E). (c) Recurrence-free survival and (d) overall survival of patients with HCC according to the MFI patterns. A log-rank test demonstrated statistically significant differences in recurrence-free and overall survival rates ($P = 0.0193$ and $P = 0.0362$, respectively). (e) Recurrence-free survival and (f) overall survival curves of the patients with HCC $\leq$4 cm. A log-rank test demonstrated statistically significant differences in the recurrence-free survival rates ($P = 0.0434$).

Table 2. Clinicopathological Findings in Patients with HCC in Relation to MFI Patterns of CEIOUS

Clinicopathological Factor	MFI Pattern: Reticular HCC (n = 26)	MFI Pattern: Thunderbolt HCC (n = 56)	P
Age, years, mean ± SD	69.5 ± 8.0	65.8 ± 9.3	0.0868
Sex, no., male:female	20:6	42:14	0.8503
Viral infection, no., HBV:HCV:non-B/C	4:12:10	9:34:13	0.3416
Background liver pathology, no.			0.5341
Normal	3	3	
Chronic hepatitis or liver fibrosis	11	22	
Liver cirrhosis	12	31	
Child-Pugh classification, no.			0.7676
A	25	53	
B	1	3	
Albumin, mg/dL, mean ± SD	4.1 ± 0.4	4.0 ± 0.5	0.6408
Total bilirubin, mg/dL, mean ± SD	0.82 ± 0.40	0.94 ± 0.40	0.2060
PT%, mean ± SD	83.3 ± 6.2	81.7 ± 8.6	0.3899
AFP, no., ≥20 ng/mL			0.0003
Yes	5	35	
No	21	21	
PIVKA-II, no., ≥40 mAU/mL			0.6779
Yes	15	35	
No	11	21	
Tumor size, cm, mean ± SD	2.6 ± 0.9	4.9 ± 3.9	0.0048
Tumor number, no., solitary:multiple	17:9	32:24	0.4788
Histological differentiation, no.			0.0004
Well/moderate	22	24	
Poor	4	32	
Tumor morphology, no.			0.1981
Simple nodular type	13	24	
Simple nodular type with extranodular growth	9	13	
Confluent multinodular type	4	19	
Tumor growth type, no.			0.0215
Expansive growth	26	46	
Infiltrative growth	0	10	
Portal vein invasion, no.			<0.0001
Negative	25	17	
Microinvasion	1	24	
Macroinvasion	0	15	
Hepatic vein invasion, no.			0.1680
Negative	24	45	
Positive	2	11	
Bile duct invasion, no.			0.1623
Negative	26	52	
Positive	0	4	
Capsule formation, no.			0.7087
Negative	8	15	
Positive	18	41	
Cancerous infiltration of the capsule, no.			0.7632
Negative	13	26	
Positive	13	30	
Formation of fibrous septum within the tumor, no.			0.3594
Negative	8	12	
Positive	18	44	
TNM stage, no., I/II:III/IV	20:6	13:43	<0.0001

Abbreviations: HBV, hepatitis B virus; HCV, hepatitis C virus; PIVKA-II, protein induced by vitamin K absence or antagosists II.

detected preoperatively using other imaging modalities (Supporting Table 1). In the 82 cases, 26 were classified as reticular HCC, and the remaining 56 cases were classified as thunderbolt HCC (Fig. 1a,b). The clinicopathological significance of the MFI patterns was then evaluated. Univariate analysis revealed that thunderbolt HCC correlated significantly

Table 3. Clinicopathological Findings in Patients with HCC in Relation to MFI Patterns of CEIOUS (Tumor Size Limited to ≤4 cm)

Clinicopathological Factor	MFI Pattern: Reticular HCC (n = 26)	MFI Pattern: Thunderbolt HCC (n = 32)	P
Age, years, mean ± SD	69.5 ± 8.0	67.5 ± 7.9	0.3548
Sex, no., male:female	20:6	22:10	0.4886
Viral infection, no., HBV:HCV:non-B/C	4:12:10	3:21:8	0.3291
Background liver pathology, no.			0.2809
Normal	3	1	
Chronic hepatitis or liver fibrosis	11	12	
Liver cirrhosis	12	19	
Child-Pugh classification, no.			0.4086
A	25	29	
B	1	3	
Albumin, mg/dL, mean ± SD	4.1 ± 0.4	4.1 ± 0.5	0.8200
Total bilirubin, mg/dL, mean ± SD	0.82 ± 0.40	0.97 ± 0.42	0.1853
PT%, mean ± SD	83.3 ± 6.2	81.0 ± 8.4	0.2383
AFP, no., ≥20 ng/mL			0.0009
Yes	5	20	
No	21	12	
PIVKA-II, no., ≥40 mAU/mL			0.5592
Yes	15	16	
No	11	16	
Tumor size, cm, mean ± SD	2.6 ± 0.9	2.9 ± 0.8	0.3004
Tumor number, no., solitary:multiple	17:9	21:11	0.9847
Histological differentiation, no.			0.0014
Well/moderate	22	14	
Poor	4	18	
Tumor morphology, no.			0.5256
Simple nodular type	13	19	
Simple nodular type with extranodular growth	9	5	
Confluent multinodular type	4	8	
Tumor growth type, no.			0.2217
Expansive growth	26	28	
Infiltrative growth	0	4	
Portal vein invasion, no.			<0.0001
Negative	25	12	
Microinvasion	1	13	
Macroinvasion	0	7	
Hepatic vein invasion, no.			0.2245
Negative	24	26	
Positive	2	6	
Bile duct invasion, no.			0.3632
Negative	26	31	
Positive	0	1	
Capsule formation, no.			0.6249
Negative	8	8	
Positive	18	24	
Cancerous infiltration of the capsule, no.			0.8128
Negative	13	17	
Positive	13	15	
Formation of fibrous septum within the tumor, no.			0.4417
Negative	8	7	
Positive	18	25	
TNM stage, no., I/II:III/IV	20:6	10:22	0.0005

Abbreviations: HBV, hepatitis B virus; HCV, hepatitis C virus; PIVKA-II, protein induced by vitamin K absence or antagosists II.

(a)

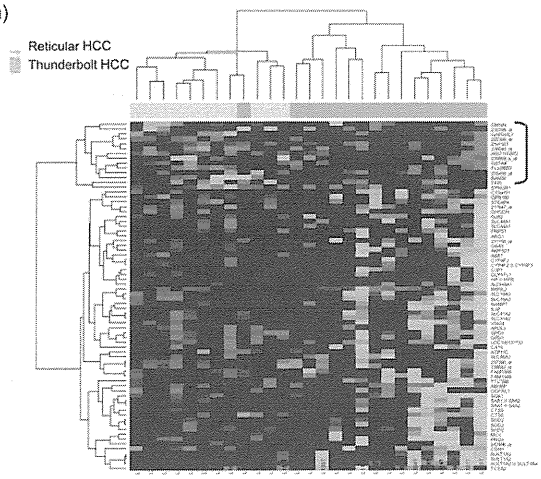

(b)

Probe set	Gene symbol	Gene title	*P value*	FC
218350_s_at	GMNN	geminin, DNA re-replication inhibitor	0.00326	2.15
230795_at	---	---	0.00392	2.10
238807_at	GAPDHL7	glyceraldehyde-3-phosphate dehydrogenase-like 7	0.00001	2.24
222366_at	---	---	0.00786	2.11
211721_s_at	ZNF551	zinc finger protein 551	0.00786	2.09
238040_at	---	---	0.00786	2.06
210387_at	HIST1H2BG	histone cluster 1, H2bg	0.00062	2.16
239069_s_at	---	---	0.00222	2.23
235405_at	GSTA4	glutathione S-transferase alpha 4	0.00665	2.04
1553145_at	FLJ39653	hypothetical FLJ39653	0.00470	2.18
235456_at	---	---	0.00392	2.13
203304_at	BAMBI	BMP and activin membrane-bound inhibitor homolog	0.00270	2.74
210665_at	TFPI	tissue factor pathway inhibitor	0.00926	2.51
210613_s_at	SYNGR1	synaptogyrin 1	0.00097	2.63

(c)

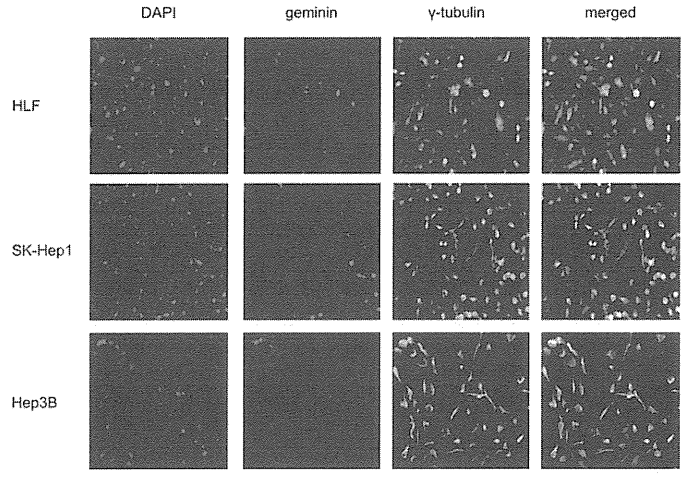

(d)

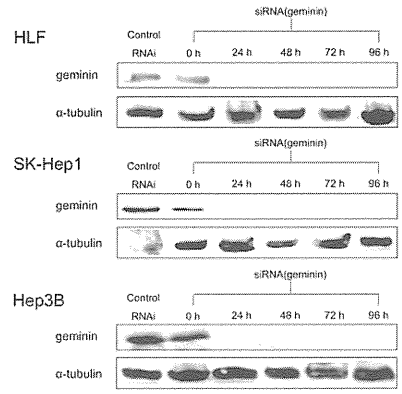

Fig. 2. Molecular and biological analysis in relation to the MFI patterns of HCC. (a) Gene expression profiling and MFI patterns. The hierarchical clustering of the gene expression (FC >2 and $P < 0.01$) in reticular HCC (blue bars) and thunderbolt HCC (orange bars). Dendrograms show the classification determined by the hierarchical clustering analysis. The red and green areas indicate relative overexpression and underexpression, respectively. (b) The differentially expressed genes in thunderbolt HCC by ranking of FC and *P* value (FC > 2, $P < 0.01$). The profiling identified geminin as one of the dominant molecules significantly overexpressed in cancer tissue of thunderbolt HCC. (c) Immunocytochemical analysis of geminin in human HCC cell lines (original magnification ×200). The predominant expression was recognized in the nucleus. DAPI, 4',6-diamidino-2-phenylindeole. (d) The silencing effects of the geminin gene. Western blot analysis confirmed that the geminin expression was markedly suppressed by the specific siRNA, compared with control siRNA (siNegative) in HLF, SK-Hep1, and Hep3B human HCC cells. (e) Growth curve analysis up after siRNA transfection. The silenced HLF, SK-Hep1 and Hep3B cells showed a significant reduction in cell proliferation. $*P <$ 0.01 versus control. The results are presented as the mean ± SD from triplicate experiments. (f) Cell cycle analyses. The percentage of <2N DNA content cells was increased in all cell lines after transfection of geminin siRNA.

with high levels of alpha-fetoprotein (AFP) ($P = 0.0003$), tumor size ($P = 0.0048$), histological dedifferentiation ($P = 0.0004$), infiltrative growth type ($P = 0.0215$), portal vein invasion ($P < 0.0001$), and tumor-node-metastasis (TNM) stage ($P < 0.0001$) (Table 2).

The recurrence-free survival and overall survival rates were then compared between the two groups. The thunderbolt HCC group demonstrated a significantly poorer prognosis than the reticular HCC group for both recurrence-free survival ($P = 0.0193$) and overall survival ($P = 0.0362$) (Fig. 1c,d). In order to exclude the bias of tumor size, we analyzed the significance of MFI patterns by limiting the tumor size to ≤4 cm in diameter. As a result, patients with thunderbolt HCC demonstrated a poorer recurrence-free survival than those with reticular HCC (Fig. 1e,f). As shown in Table 3, thunderbolt HCC also correlated significantly with high levels of AFP, histological dedifferentiation, portal vein invasion, and TNM stage, even if the tumor size was ≤4 cm.

Genome-wide Gene Expression Analysis Correlated to the MFI Patterns of Human HCC. Gene expression was analyzed in 27 samples of HCC,

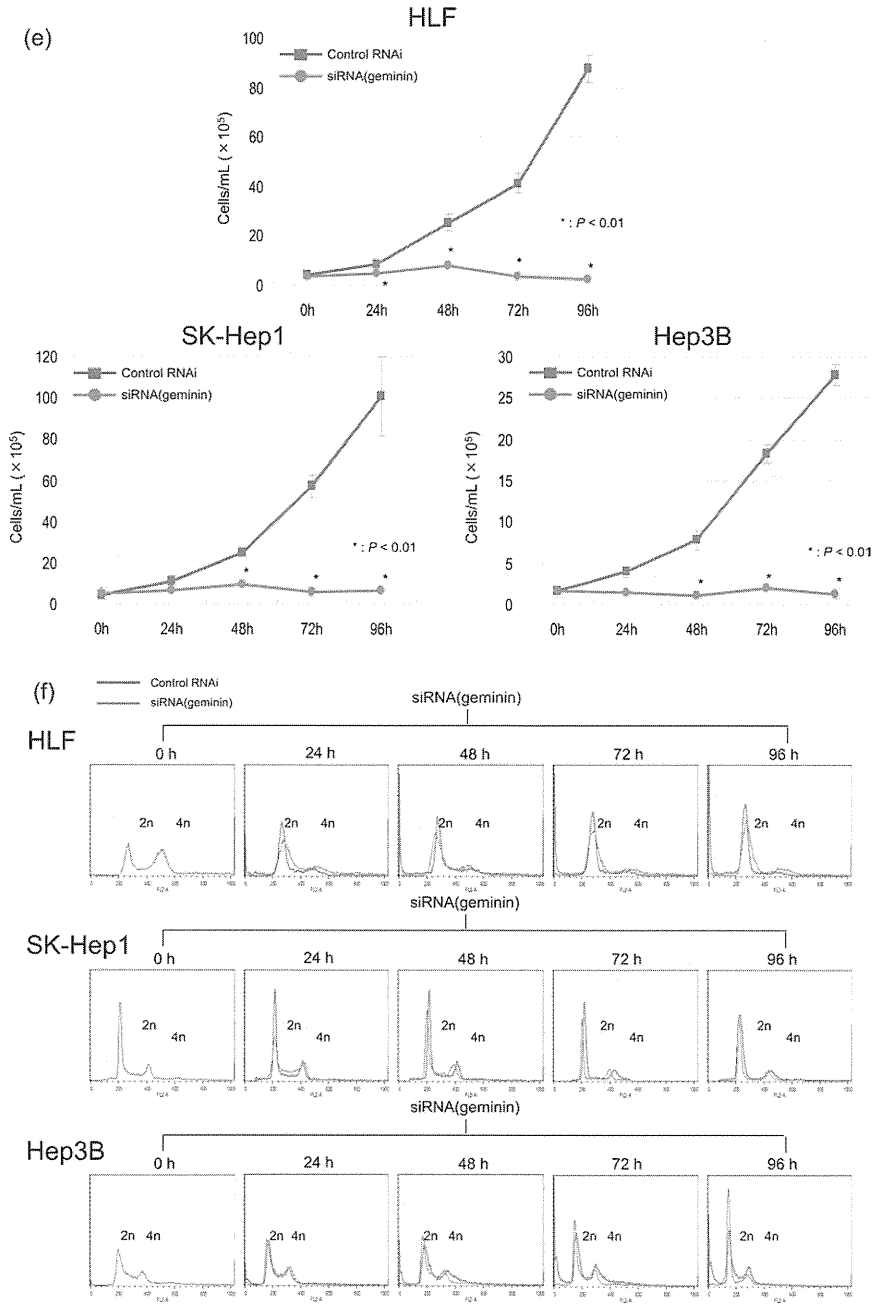

Fig. 2. (Continued)

including 11 reticular HCCs and 16 thunderbolt HCCs. The gene expression changes in 72 probe sets were evaluated by microarray analysis in 27 HCCs (FC >2, $P < 0.01$). As shown in Fig. 2a, the hierarchical clustering clearly divided the samples, and 14 genes were up-regulated in thunderbolt HCC. As displayed in Fig. 2b, in order of the FC and P values, a rereplication inhibitor geminin was significantly overexpressed in thunderbolt HCCs.

Significance of Geminin Expression in Human HCC Cells. The expression of the geminin protein was then analyzed in human HCC cell lines. The protein expression was recognized by western blotting in all of eight cell lines examined. Among them, we selected the three cell lines according to the expression level of geminin (HLF, high; SK-Hep1, moderate; Hep3B, low). Immunocytochemical analysis in these cell lines showed the potent expression of geminin protein, mainly in the nucleus (Fig. 2c). Next, the effects of the specific siRNAs against geminin were assessed in the HCC cell lines (HLF, SK-Hep1, and Hep3B). Western blot analysis certified that the expression of geminin was markedly silenced by the specific siRNA, but not by the control siRNA (Fig. 2d).

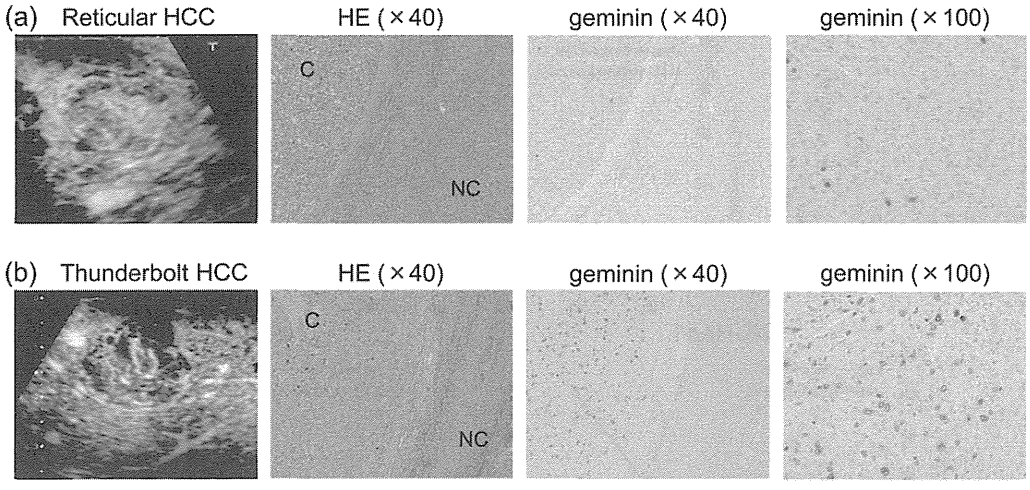

(c)

	Reticular HCC (n = 26)	Thunderbolt HCC (n = 26)	*P* value
geminin positive cells rate(%)	3.1 ± 0.6 (0.2 - 13.6)	9.3 ± 0.9 (0.6 - 32.1)	**< 0.0001**
geminin			**< 0.0001**
(-) (< 5%)	22	15	
(+) (≥ 5%, < 10%)	3	19	
(++) (≥ 10%)	1	22	

Fig. 3. Immunohistochemical analysis of expression of geminin protein in cancer tissues (C) and noncancerous tissues (NC) of human HCC. Compared with the cancer tissue of reticular HCC (a), the expression of geminin protein was increased in the cancer tissue of thunderbolt HCC (b). In noncancerous tissue of HCC, the expression of geminin was not detected. (c) Mean percentages of geminin-positive cells in cancer tissues (upper) and the case numbers of each type HCC (lower).

As shown in the cell growth assays of HCC (Fig. 2e), geminin siRNA significantly depressed cellular proliferation 96 hours after transfection, compared with cells treated with control siRNA ($P < 0.01$). In addition, cell cycle analysis demonstrated the accumulation of <2N DNA content in all of the cell lines after transfection of geminin siRNA (Fig. 2f). These results suggest that geminin has an essential role in the cell cycling of human HCC.

MFI Pattern of HCC Tumors and the Expression of Geminin Protein. Immunohistochemical validation of geminin protein was then performed using 82 tissue samples of HCC. As a shown in Fig. 3, the geminin protein stained mainly in the nucleus was clearly detected in cancer cells of HCC, but not in noncancerous liver tissue. The frequency of geminin-positive cancer cells was 9.3% in thunderbolt HCCs, but only 3.1% in reticular HCCs, indicating the statistical significance between the two types ($P < 0.0001$). The statistical significance was also observed even if the tumor size was limited (Supporting Table 3). The geminin expression and MFI patterns were not associated with cholangiocellular differentiation as well as progenitor cell markers (Supporting Fig. 1). According to the multivariate analysis for the MFI patterns of HCC using logistic regression mode, the expression of geminin protein ($P = 0.0180$), tumor size ($P = 0.0222$), and portal vein invasion ($P = 0.0174$) were statistically independent factors of MFI thunderbolt HCC (Table 4).

Postoperative Outcomes of HCC Patients and the Expression of Geminin Protein. The clinicopathological significance of geminin expression was then evaluated in the 82 patients enrolled in this study (Table 5). The univariate analysis for overall survival

Table 4. Multivariate Analysis for Independent Predictors of MFI Patterns of HCC

Clinicopathological Factor	HR (95% CI)	*P*
AFP, ≥20 ng/mL	3.276 (0.464-23.145)	0.2342
Tumor size, cm	3.704 (1.206-11.378)	0.0222
Histological differentiation		
Well/moderate:poor	6.082 (0.669-55.320)	0.1090
Tumor growth type		
Eg:Ig	NA	0.9813
Portal vein invasion		
Negative:Positive	43.968 (1.945-993.935)	0.0174
TNM stage (I/II:III/IV)	4.341 (0.287-65.582)	0.2892
Geminin	1.289 (1.044-1.590)	0.0180

CI, confidence interval; Eg, expansive growth; HR, hazard ratio; Ig, infiltrative growth; NA, not applicable.

Table 5. Univariate and Multivariate Analysis of Overall Survival

	Univariate Analysis		Multivariate Analysis	
Clinicopathological Factor	**HR (95% CI)**	***P***	**HR (95% CI)**	***P***
Age, years	1.026 (0.972-1.083)	0.3745		
Sex, male versus female	1.333 (0.441-4.034)	0.6107		
Viral infection		0.8216		
HBV	1.814 (0.408-8.076)			
HCV	0.456 (0.168-1.297)			
Non-B/C	1.703 (0.556-5.124)			
Background liver pathology		0.5585		
Normal	0.635 (0.145-2.780)			
Chronic hepatitis or liver fibrosis	0.949 (0.371-2.430)			
Liver cirrhosis	1.218 (0.488-3.040)			
Child-Pugh classification, A versus B	2.246 (0.516-9.784)	0.2810		
Albumin	0.355 (0.150-0.842)	0.0187	0.619 (0.213-1.804)	0.3797
PT%	0.969 (0.921-1.019)	0.2205		
Total bilirubin	0.894 (0.293-2.728)	0.8446		
AFP, ng/mL, $\geq$20 versus <20	4.562 (1.511-13.771)	0.0071	1.780 (0.484-6.555)	0.3856
PIVKA-II, mAU/mL, $\geq$40 versus < 40	1.856 (0.668-5.160)	0.2357		
Tumor size, cm	1.035 (0.978-1.157)	0.1510		
Tumor number, solitary versus multiple	2.930 (1.151-7.462)	0.0242	2.254 (0.607-8.371)	0.2247
Histological differentiation, well/moderate versus poor	3.327 (1.276-8.677)	0.0140	1.137 (0.303-4.259)	0.8492
Tumor morphology, SN/SNEG versus CM	2.178 (0.895-5.299)	0.0863		
Tumor growth type, Eg versus Ig	3.636 (1.374-9.624)	0.0093	2.588 (0.664-10.088)	0.1706
Portal vein invasion	2.183 (0.869-5.481)	0.0965		
Hepatic vein invasion	4.140 (1.621-10.575)	0.0030	5.039 (1.441-17.627)	0.0113
Bile duct invasion	2.103 (0.273-16.217)	0.4757		
Capsule formation	1.571 (0.168-3.996)	0.3427		
Cancerous infiltration of the capsule	1.455 (0.584-3.624)	0.4205		
Formation of fibrous septum within the tumor	1.251 (0.415-3.778)	0.6907		
TNM stage, I/II versus III/IV	3.392 (1.129-10.186)	0.0295	1.332 (0.255-6.965)	0.7339
Geminin	1.120 (1.053-1.192)	0.0003	1.098 (1.017-1.185)	0.0170

CI, confidence interval; CM, confluent multinodular type; Eg, expansive growth; HBV, hepatitis B virus; HCV, hepatitis C virus; HR, hazard ratio; Ig, infiltrative growth; PIVKA-II, protein induced by vitamin K absence or antagosists II; SN, simple nodular type; SNEG, simple nodular type with extranodular growth.

of HCC revealed that the expression of geminin protein ($P = 0.0003$), serum level of albumin ($P = 0.0187$) and AFP ($P = 0.0071$), tumor number ($P = 0.0242$), histological dedifferentiation ($P = 0.0140$), infiltrative growth type ($P = 0.0093$), hepatic vein invasion ($P = 0.0030$), and TNM stage ($P = 0.0074$) were significantly for overall survival of HCC. The multivariate analysis revealed that the expression of geminin protein ($P = 0.0170$) and hepatic vein invasion ($P = 0.0113$) were statistically independent factors of overall survival.

Discussion

Tumor angiogenesis is one of the special features of HCC progression, and the detection of abnormal vasculature in a focal liver lesion aids in the identification of HCC.[14,15,18-21] Previous studies have reported that contrast-enhanced ultrasonography using microbubble-based contrast agents is useful for visualizing the vasculature of HCC.[22,23] In particular, the difference in vasculature of HCC and surrounding liver could be evaluated in detail using MFI with contrast agents.[23,34] Although some studies reported that CEIOUS was useful for detection of focal HCC lesions during hepatic resection, the significance of CEIOUS findings of MFI has not yet been clarified.[35,36]

In this study, we investigated the MFI with Sonazoid CEIOUS in hepatic resection for HCC. The MFI pattern was classified as reticular HCC and thunderbolt HCC, and as shown in Table 2 and Fig. 1c,d, thunderbolt HCC was significantly associated with the advanced progression and poor prognosis. We also revealed that the thunderbolt pattern was useful to predict the microinvasion into portal veins, which were undetectable by preoperative imaging modalities (Table 2). A subgroup analysis limiting the tumor size to $\leq$4 cm also demonstrated advanced progression and poorer prognosis in thunderbolt HCC compared with reticular HCC (Fig. 1e,f and Table 3). Additionally, we found the clinicopathological differences between each MFI pattern even when the tumor size was limited to <3 cm or <5 cm (Supporting Table 2).

To clarify the molecular and biological features associated with the MFI patterns, the gene expression profiling was further evaluated in human HCC

samples (Fig. 2a). The gene expression analysis identified geminin as one of the dominant molecules significantly overexpressed in thunderbolt HCC tissue (Fig. 2b). Geminin is known as a DNA rereplication inhibitor that is expressed in the G2, S, and M phases but not in the G0 and G1 phases.[37,38] DNA replication begins with assembly of prereplication complexes (preRCs) at multiple sites throughout the genome as cells exit metaphase.[39] preRCs are then assembled into preinitiation complexes that are subsequently activated by protein kinases to begin DNA synthesis (S phase). Once S phase begins, further assembly of preRCs is prevented by phosphorylation, ubiquitination, and degradation of preRC proteins ORC1, CDC6, and CDT1, and by geminin, a specific protein inhibitor of CDT1 activity unique to metazoan.[40,41]

Previous studies have reported that geminin is specifically expressed in proliferating cells, including lymphocytes, crypt epithelial cells, and sperm cells, but not in nonproliferating epithelial cells, including normal neurocytes, muscle cells, and hepatocytes.[42,43] As for malignant neoplasms, the overexpression of geminin was reported in advanced human cancers such as breast, lung, renal, and colorectal carcinomas.[41,44-48] According to our additional analysis, Ki67 expression was significantly associated with geminin expression ($P = 0.0112$), supporting the proliferative role of geminin in HCC (Supporting Fig. 2). Indeed, *in vitro* knockdown of geminin significantly suppressed the cell proliferation of human HCC cell lines (Fig. 2d-f).

Our immunohistochemical analysis on clinical samples clarified that the frequency of geminin-positive cancer cells correlated significantly with thunderbolt HCCs (Fig. 3 and Supporting Table 3). In addition, the clinical significance of geminin was noted in the overall survival (Table 5). Quaglia et al.[49] reported that the expression level of geminin was increased from regenerative and dysplastic nodules to HCC nodules, indicating its potential association with hepatocarcinogenesis. The molecular and biological role of geminin in HCC progression should be studied further.

In conclusion, the intraoperative MFI patterns were independent predictors of HCC progression, resulting in poor prognosis of the patients. Such vascular patterns were distinctly identified by gene expression profiling, such as geminin, which might play roles in HCC cell proliferation. Application of CEIOUS might be useful in determining the postoperative treatment of HCC. Additional studies should clarify the clinical impacts of CEIOUS MFI patterns.

Reference

1. Parkin DM, Bray F, Ferlay J, Pisani P. Estimating the world cancer burden: Globocan 2000. Int J Cancer 2001;94:153-156.
2. Hashem B, El-Serag. Hepatocellular carcinoma. N Engl J Med 2011; 365:1118-1127.
3. Cha CH, Saif MW, Yamane BH, Weber SM. Hepatocellular carcinoma: current management. Curr Probl Surg 2010;47:10-67.
4. Arii S, Yamaoka Y, Futagawa S, Inoue K, Kobayashi K, Kojiro M, et al. Results of surgical and nonsurgical treatment for small-sized hepatocellular carcinomas: a retrospective and nationwide survey in Japan. The Liver Cancer Study Group of Japan. HEPATOLOGY 2000;32: 1224-1229.
5. Hanish SI, Knechtle SJ. Liver transplantation for the treatment of hepatocellular carcinoma. Oncology (Williston Park) 2011;25:752-757.
6. Kruskal JB, Kane RA. Intraoperative US of the liver: techniques and clinical applications. Radiographics 2006;26:1067-1084.
7. Postema M, Gilja OH. Contrast-enhanced and targeted ultrasound. World J Gastroenterol 2011;17:28-41.
8. Sontum PC. Physicochemical characteristics of Sonazoid, a new contrast agent for ultrasound imaging. Ultrasound Med Biol 2008;34: 824-833.
9. Watanabe R, Matsumura M, Chen CJ, Kaneda Y, Ishihara M, Fujimaki M. Gray-scale liver enhancement with Sonazoid (NC100100), a novel ultrasound contrast agent; detection of hepatic tumors in a rabbit model. Biol Pharm Bull 2003;26:1272-1277.
10. Mandai M, Koda M, Matono T, Nagahara T, Sugihara T, Ueki M, et al. Assessment of hepatocellular carcinoma by contrast-enhanced ultrasound with perfluorobutane microbubbles: comparison with dynamic CT. Br J Radiol 2011;84:499-507.
11. Goto E, Masuzaki R, Tateishi R, Kondo Y, Imamura J, Goto T, et al. Value of post-vascular phase (Kupffer imaging) by contrast-enhanced ultrasonography using Sonazoid in the detection of hepatocellular carcinoma. J Gastroenterol 2012;47:477-485.
12. Sugimoto K, Shiraishi J, Moriyasu F, Saito K, Doi K. Improved detection of hepatic metastases with contrast-enhanced low mechanical-index pulse inversion ultrasonography during the liver-specific phase of sonazoid: observer performance study with JAFROC analysis. Acad Radiol 2009;16:798-809.
13. Mitsunori Y, Tanaka S, Nakamura N, Ban D, Irie T, Noguchi N, et al. Contrast-enhanced intraoperative ultrasound for hepatocellular carcinoma: high sensitivity of diagnosis and therapeutic impact. J Hepatobiliary Pancreat Sci 2012; doi:10.1007/s00534-012-0507-9.
14. Carmeliet P, Jain RK. Angiogenesis in cancer and other diseases. Nature 2000;407:249-257.
15. Carmeliet P, Jain RK. Molecular mechanisms and clinical applications of angiogenesis. Nature 2011;473:298-307.
16. Eberhard A, Kahlert S, Goede V, Hemmerlein B, Plate KH, Augustin HG. Heterogeneity of angiogenesis and blood vessel maturation in human tumors: implications for antiangiogenic tumor therapies. Cancer Res 2000;60:1388-1393.
17. Baish JW, Jain RK. Fractals and cancer. Cancer Res 2000;60: 3683-3688.
18. Tanaka S, Arii S. Current status and perspective of antiangiogenic therapy for cancer: hepatocellular carcinoma. Int J Clin Oncol 2006;11: 82-89.
19. Llovet JM, Ricci S, Mazzaferro V, Hilgard P, Gane E, Blanc JF, et al; SHARP Investigators Study Group. Sorafenib in advanced hepatocellular carcinoma. N Engl J Med 2008;359:378-390.
20. Tanaka S, Sugimachi K, Yamashita Yi Y, Ohga T, Shirabe K, Shimada M, Wands JR, et al. Tie2 vascular endothelial receptor expression and function in hepatocellular carcinoma. HEPATOLOGY 2002;35: 861-867.
21. Toyoda H, Fukuda Y, Hayakawa T, Kumada T, Nakano S. Changes in blood supply in small hepatocellular carcinoma: correlation of angiographic images and immunohistochemical findings. J Hepatol 1997;27: 654-660.

22. Ogawa S, Kumada T, Toyoda H, Ichikawa H, Kawachi T, Otobe K, et al. Evaluation of pathological features of hepatocellular carcinoma by contrast-enhanced ultrasonography: comparison with pathology on resected specimen. Eur J Radiol 2006;59:74-81.
23. Sugimoto K, Moriyasu F, Kamiyama N, Metoki R, Yamada M, Imai Y, et al. Analysis of morphological vascular changes of hepatocellular carcinoma by microflow imaging using contrast-enhanced sonography. Hepatol Res 2008;38:790-799.
24. Asayama Y, Yoshimitsu K, Nishihara Y, Irie H, Aishima S, Taketomi A, et al. Arterial blood supply of hepatocellular carcinoma and histologic grading: radiologic-pathologic correlation. AJR Am J Roentgenol 2008;190:28-34.
25. Tarhan NC, Hatipoğlu T, Ercan E, Bener M, Keleş G, Başaran C, et al. Correlation of dynamic multidetector CT findings with pathological grades of hepatocellular carcinoma. Diagn Interv Radiol 2011;17:328-333.
26. Quackenbush J. Microarray analysis and tumor classification. N Engl J Med 2006;354:2463-2472.
27. Hoshida Y, Villanueva A, Kobayashi M, Peix J, Chiang DY, Camargo A, et al. Gene expression in fixed tissues and outcome in hepatocellular carcinoma. N Engl J Med 2008;359:1995-2004.
28. Aihara A, Tanaka S, Yasen M, Matsumura S, Mitsunori Y, Murakata A, et al. The selective Aurora B kinase inhibitor AZD1152 as a novel treatment for hepatocellular carcinoma. J Hepatol 2010;52:63-71.
29. Murakata A, Tanaka S, Mogushi K, Yasen M, Noguchi N, Irie T, et al. Gene expression signature of the gross morphology in hepatocellular carcinoma. Ann Surg 2011;253:94-100.
30. Yoshitake K, Tanaka S, Mogushi K, Aihara A, Murakata A, Matsumura S, et al. Importin-α1 as a novel prognostic target for hepatocellular carcinoma. Ann Surg Oncol 2011;18:2093-2103.
31. Tanaka S, Arii S, Yasen M, Mogushi K, Su NT, Zhao C, et al. Aurora kinase B is a predictive factor for the aggressive recurrence of hepatocellular carcinoma after curative hepatectomy. Br J Surg 2008;95:611-619.
32. Liver Cancer Study Group of Japan. The general rules for the clinical and pathological study of primary liver cancer. 3rd ed. Tokyo; 2010.
33. Tanaka S, Pero SC, Taguchi K, Shimada M, Mori M, Krag DN, et al. Specific peptide ligand for Grb7 signal transduction protein and pancreatic cancer metastasis. J Natl Cancer Inst 2006;98:491-498.
34. Sugimoto K, Shiraishi J, Moriyasu F, Ichimura S, Metoki R, Doi K. Analysis of intrahepatic vascular morphological changes of chronic liver disease for assessment of liver fibrosis stages by micro-flow imaging with contrast-enhanced ultrasound: preliminary experience. Eur Radiol 2010;20:2749-2757.
35. Nanashima A, Tobinaga S, Abo T, Kunizaki M, Takeshita H, Hidaka S, et al. Usefulness of sonazoid-ultrasonography during hepatectomy in patients with liver tumors: a preliminary study. J Surg Oncol 2011; 103:152-157.
36. Arita J, Takahashi M, Hata S, Shindoh J, Beck Y, Sugawara Y, et al. Usefulness of contrast-enhanced intraoperative ultrasound using sonazoid in patients with hepatocellular carcinoma. Ann Surg 2011;254: 992-999.
37. Xouri G, Dimaki M, Bastiaens PI, Lygerou Z. Cdt1 interactions in the licensing process: a model for dynamic spatiotemporal control of licensing. Cell Cycle 2007;6:1549-1552.
38. Karamitros D, Kotantaki P, Lygerou Z, Veiga-Fernandes H, Pachnis V, Kioussis D, et al. Life without geminin. Cell Cycle 2010;9:3181-3185.
39. Noguchi K, Vassilev A, Ghosh S, Yates JL, DePamphilis ML. The BAH domain facilitates the ability of human Orc1 protein to activate replication origins in vivo. EMBO J 2006;25:5372-5382.
40. DePamphilis ML, Blow JJ, Ghosh S, Saha T, Noguchi K, Vassilev A. Regulating the licensing of DNA replication origins in metazoa. Curr Opin Cell Biol 2006;18:231-239.
41. Blow JJ, Gillespie PJ. Replication licensing and cancer—a fatal entanglement? Nat Rev Cancer 2008;8:799-806.
42. Wohlschlegel JA, Kutok JL, Weng AP, Dutta A. Expression of geminin as a marker of cell proliferation in normal tissues and malignancies. Am J Pathol 2002;161:267-273.
43. Eward KL, Obermann EC, Shreeram S, Loddo M, Fanshawe T, Williams C, et al. DNA replication licensing in somatic and germ cells. J Cell Sci 2004;117:5875-5886.
44. Gonzalez MA, Tachibana KE, Chin SF, Callagy G, Madine MA, Vowler SL, et al. Geminin predicts adverse clinical outcome in breast cancer by reflecting cell-cycle progression. J Pathol 2004;204:121-130.
45. Dudderidge TJ, Stoeber K, Loddo M, Atkinson G, Fanshawe T, Griffiths DF, et al. Mcm2, Geminin, and KI67 define proliferative state and are prognostic markers in renal cell carcinoma. Clin Cancer Res 2005;11:2510-2517.
46. Nishihara K, Shomori K, Tamura T, Fujioka S, Ogawa T, Ito H. Immunohistochemical expression of geminin in colorectal cancer: implication of prognostic significance. Oncol Rep 2009;21:1189-1195.
47. Haruki T, Shomori K, Hamamoto Y, Taniguchi Y, Nakamura H, Ito H. Geminin expression in small lung adenocarcinomas: implication of prognostic significance. Lung Cancer 2011;71:356-362.
48. Zhu W, Depamphilis ML. Selective killing of cancer cells by suppression of geminin activity. Cancer Res 2009;69:4870-4877.
49. Quaglia A, McStay M, Stoeber K, Loddo M, Caplin M, Fanshawe T, et al. Novel markers of cell kinetics to evaluate progression from cirrhosis to hepatocellular carcinoma. Liver Int 2006;26:424-432.

HEPATOLOGY
Official Journal of the American Association for the Study of Liver Diseases

Visualization of Stem Cell Features in Human Hepatocellular Carcinoma Reveals *In Vivo* Significance of Tumor-Host Interaction and Clinical Course

Shunsuke Muramatsu,[1] Shinji Tanaka,[1] Kaoru Mogushi,[2] Rama Adikrisna,[1] Arihiro Aihara,[1] Daisuke Ban,[1] Takanori Ochiai,[1] Takumi Irie,[1] Atsushi Kudo,[1] Noriaki Nakamura,[1] Koh Nakayama,[3] Hiroshi Tanaka,[2] Shoji Yamaoka,[4] and Shigeki Arii[1]

Hepatocellular carcinoma (HCC) is one of the most aggressive malignancies because of recurrence and/or metastasis even after curative resection. Emerging evidence suggests that tumor metastasis and recurrence might be driven by a small subpopulation of stemness cells, so-called cancer stem cells (CSCs). Previous investigations have revealed that glioma and breast CSCs exhibit intrinsically low proteasome activity and that breast CSCs also reportedly contain a lower reactive oxygen species (ROS) level than corresponding nontumorigenic cells. Here we visualized two stem cell features, low proteasome activity and low intracellular ROS, in HCC cells using two-color fluorescence activated cell sorting to isolate cells with stem cell features. These cells were then analyzed for their division behavior in normoxia and hypoxia, expression of stem cell markers, tumorigenicity, metastatic potential, specific gene expression signatures, and their clinical implications. A visualized small subpopulation of HCC cells demonstrated asymmetric divisions. Their remarkable tumorigenicity in nonobese diabetic/severe combined immunodeficient mice suggested the cancer initiation potential of these HCC CSCs. Comprehensive gene expression analysis revealed that chemokine-related genes were up-regulated in the CSCs subpopulation. Our identified HCC CSCs facilitated the migration of macrophages *in vitro* and demonstrated metastatic potential by way of recruitment of macrophages *in vivo*. In patients who undergo curative operation for HCC, the CSC-specific gene signature in the liver microenvironment significantly correlates with recurrence. *Conclusion*: Based on these findings, the stem cell feature monitoring system proposed here is a promising tool to analyze the *in vivo* significance of CSC microenvironments in human HCCs. (HEPATOLOGY 2013;58:218-228)

Hepatocellular carcinoma (HCC) is one of the most common malignancies and the third leading cause of cancer death worldwide.[1] The primary curative treatment for HCC is surgical resection; however, even after curative resection patient prognosis remains poor because of frequent recurrence and/or metastasis.[2,3] Because cancer stem cells (CSCs) possess self-renewal capacity, multilineage potency, and increased tumorigenicity, it has been hypothesized that CSCs exist as a small population within the bulk tumors and play a critical role in cancer progression, metastasis, and recurrence.[4] Various tools have been reported for identification of the CSC population, including the cell surface markers CD44, CD133, CD90, and ESA/EpCAM.[5-8] In addition, specific stemness properties based on stem cell biology of their

Abbreviations: CSC, cancer stem cells; FDR, false discovery rate; GSEA, gene set enrichment analysis; HCC, hepatocellular carcinoma; NOD/SCID, nonobese diabetic / severe combined immunodeficient; ODC, ornithine decarboxylase; ROS, reactive oxygen species.

From the [1]Department of Hepato-Biliary-Pancreatic Surgery, Graduate School of Medicine, Tokyo Medical and Dental University, Tokyo, Japan; [2]Department of Computational Biology, Graduate School, Tokyo Medical and Dental University, Tokyo, Japan; [3]Oxygen Biology Unit, Frontier Research Laboratory, Medical Research Institute Tokyo Medical and Dental University, Tokyo, Japan; [4]Department of Molecular Virology, Tokyo Medical and Dental University, Tokyo, Japan.

Received June 30, 2012; accepted February 13, 2013.

Supported by Grant-in-Aid for Scientific Research on Innovative Areas, Scientific Research (A), Project of Development of Innovative Research on Cancer Therapeutics from Ministry of Education, Culture, Sports, Science & Technology of Japan, and Health & Labour Sciences Research Grant from Ministry of Health Labour & Welfare of Japan.

intracellular activities may be useful in identifying CSCs.[9] For example, one property that may be useful in identifying stemness is 26S proteasome activity, which is involved in a diverse array of biological processes, including cell-cycle progression, DNA repair, apoptosis, and protein quality control.[10] Proteasome activity is significantly activated in cancer cells with proliferating and hypermetabolic activities, but generally suppressed in dormant states of stem cells.[11] Vlashi et al.[12] reported that human glioma and breast CSCs were identical to the subpopulation of cells monitored by green fluorescent protein ZsGreen fused to a degron motif of ornithine decarboxylase (ODC), which accumulated within the cell because of low 26S proteasome activity. Stem cells are also characterized by resistance to oxidative stress (superoxide) according to data obtained using the detoxifier system.[13] Hematopoietic stem cells contain a lower level of reactive oxygen species (ROS) than their mature progeny, and these differences are critical for maintaining stem cell function.[14] Human breast CSCs contain lower ROS levels, especially mitochondrial superoxide, than corresponding nontumorigenic cells.[15] In this study, we visualized two stem cell features, low proteasome activity and low ROS levels, in human HCC cells using the ZsGreen-fused degron sequence of ODC and the mitochondrial superoxide indicator MitoSOX Red, respectively. This monitoring system of stemness is a promising tool to elucidate the mechanism of progression and metastasis of human HCC.

Materials and Methods

Cell Culture. HCC cell lines (Hep3B, SK-Hep1, HuH7, and HLF) were purchased from the American Type Culture Collection (Manassas, VA) and the Human Science Research Resources Bank (Osaka, Japan). HuH7, Hep3B, and SK-Hep1 cells were cultured in log-growth phase in 1640 RPMI medium (Invitrogen, Carlsbad, CA), supplemented with 10% fetal bovine serum (Sigma-Aldrich, St. Louis, MO) and Pen/Strep (Sigma) as antibiotics. HLF cells were cultured in Dulbecco's modified Eagle's medium (DMEM; Invitrogen, Carlsbad, CA), supplemented with 10% fetal bovine serum and Pen/Strep, and grown in an incubator with 5% CO_2 at 37°C. Four HCC tumor samples were harvested at the time of surgery. After digestion with type IV collagenase (100 units/mL; Sigma) at 37°C for 15 minutes, the tissues were minced and the cell suspension was passed through a 100-μM nylon mesh and placed into DMEM medium. Cells were cultured in log-growth phase in DMEM medium (Invitrogen), supplemented with 10% fetal bovine serum (Sigma) and grown in an incubator with 5% CO_2 at 37°C.

Retroviral Transduction of the Degron Reporter Into Human HCC Cells. The degron sequence of ODC is known to be directly recognized by the proteasome, which leads to the immediate destruction of the involved protein. A retroviral expression vector pQCXIN-ZsGreen-cODC, containing green fluorescent ZsGreen-labeled degron ODC (Gdeg), was kindly provided by Dr. Frank Pajonk. The vector was transfected into platinum retroviral packaging cells and the retrovirus collected from the supernatant was used to infect HCC cells. Stable transfectants were selected with G418 (Invitrogen), and the accumulation of ZsGreen-degron ODC protein (Gdeg) was monitored by fluorescence microscopy and flow cytometry (FITC channel). Stable transfection was confirmed by exposing the cells to the proteasome inhibitor MG-132 (Calbiochem, San Diego, CA) for 12 hours. The established cell lines (HuH7, Hep3B, HLF, and SK-Hep1) as well as one cell culture line derived from each of the four HCC tissues were successfully engineered to stably express Gdeg. Fluorescence microscopy was performed using Axio-Observer (Carl Zeiss, Oberkochen, Germany), and images were acquired digitally using AxioVision (Carl Zeiss).

Flow Cytometry and Cell Sorting. For the flow cytometry experiments the cell number was evaluated using a FACSCanto II (BD Biosciences), and cell sorting was performed using a FACSAria II (BD Biosciences). HCC cells were washed with phosphate-buffered saline (PBS), then enzymatically dissociated using 0.05% trypsin-EDTA (Invitrogen). Trypsinized cells were suspended in fluorescence activated cell sorting (FACS) buffer and analyzed on a FACSCanto II using FACSDiva software (BD Biosciences). For intracellular ROS analysis, cells were loaded with 5 mM MitoSOX

Address reprint requests to: Shinji Tanaka, M.D., Ph.D., FACS, Department of Hepato-Biliary-Pancreatic Surgery, Graduate School of Medicine, Tokyo Medical and Dental University, 1-5-45 Yushima, Bunkyo-ku, Tokyo 113-8519, Japan. E-mail: shinji.msrg@tmd.ac.jp; fax: +81-3-5803-0263.

View this article online at wileyonlinelibrary.com.
DOI 10.1002/hep.26345
Potential conflict of interest: Nothing to report.
Additional Supporting Information may be found in the online version of this article.

Red (Invitrogen) at 37°C for 30 minutes and were immediately analyzed using FACSCanto II. $Gdeg^{high}ROS^{low}$ cells represented 0.16%-2.5% of the established HCC cell lines (Supporting Table 1). The percentage of $Gdeg^{high}ROS^{low}$ cells remained the same immediately after isolation by FACS, but increased to approximately 40% after time in culture (Supporting Fig. 4). For surface maker analysis, cells were labeled with allophycocyanin-conjugated antihuman CD44, CD90, EpCAM (BioLegend), and CD133/1 (MACS Miltenyi Biotec) antibodies. Labeled cells were immediately analyzed using FACSCanto II.

Time-Lapse Analysis. After FACS, $Gdeg^{high}$ or $Gdeg^{low}$ HCC cells were plated separately at a density of 10^4 cells in 6-cm dishes and in log-growth phase in 1640 RPMI medium (Invitrogen), supplemented with 10% fetal bovine serum (Sigma) and Pen/Strep (Sigma) as antibiotics. After incubation in 5% CO_2 at 37°C overnight, cell attachment was confirmed. Image analysis was performed using AxioVision and AxioObserver.

Treatment With Hypoxia or $CoCl_2$. HCC cells were exposed to hypoxic conditions (1% O_2, 5% CO_2, and 94% N_2) in an anaerobic workstation (Hirasawa Works, Tokyo, Japan). Oxygen concentration inside the workstation was constantly monitored by the oxygen sensor (MC-8G-S, Iijima Electrics, Gamagori, Japan) and maintained at 1% during the experiment. Cells (2.5×10^5) were grown with RPMI medium plus 3.5 g/L D-glucose in 10-cm dishes. The proportion of fluorescent cells was measured using FACSCanto II every 2 days. Cells were passaged every 6 days in an anaerobic workstation.

To further assess the effect of hypoxia on HCC cells, cells were treated with 100 μM $CoCl_2$ (Sigma) and/or 10 nM echinomycin (Sigma) added to the medium. After 24 and 48 hours, the proportion of fluorescence cells was measured using FACSCanto II. Chemosensitivity to the anticancer drug fluorouracil (5-FU) was analyzed using $Gdeg^{high}$ HuH7 and unsorted HuH7 cells under these hypoxia-mimicking condition. 5-FU was suspended in the culture media, serially diluted across 96-well microtiter plates (100 μL), and incubated at 37°C with 5% CO_2 for 48 hours. The number of living cells was measured using the MTS assay (Celltiter-Glo Luminescent Cell Viability Assay, Promega, Madison, WI), according to the manufacturer's instructions. The absorbance was read at 490 nm using a multiwell plate reader (Model 550, Bio-Rad, Richmond, CA), with wells containing medium but no cells serving as blank controls. Experiments were independently evaluated in triplicate.

Spheroid Assay. The spheroid assay was performed as described.[16] After FACS, $Gdeg^{high}$ or unsorted cells were plated separately at a density of 1,000 cells in low attachment plates (96-well Ultra Low Cluster Plate; Costar, Corning, NY) and incubated in serum-free DMEM/F12 medium (Invitrogen). For observation by time-lapse microscopy, 6-cm dishes were coated with poly-HEMA (20 mg/mL; Sigma). Image analysis was performed using AxioVision and AxioObserver.

Tumor Xenotransplantation and Tumorigenicity. Female NOD.CB17-$PRkdc^{Scid}$/J mice aged 4-6 weeks were purchased from Charles River Japan (Kanagawa, Japan). Various numbers of sorted $Gdeg^{high}ROS^{low}$ and unsorted HCC cells, ranging from 1×10^2 to 1×10^5 cells, were each mixed with 100 μL of Matrigel (BD Biosciences) and injected subcutaneously into both flanks of mice under anesthesia. Tumor formation was monitored every 2 days. All *in vivo* procedures were approved by the Animal Care Committee of Tokyo Medical and Dental University (Permission No. 090235).

RNA Extraction and Gene Expression Analysis. Total RNA was extracted from cancer and adjacent noncancerous tissues using the RNeasy kit (Qiagen, Hilden, Germany), and the integrity of obtained RNA was assessed using the Agilent 2100 Bioanalyzer (Agilent Technologies, Palo Alto, CA). All samples had an RNA Integrity Number greater than 5.0. Contaminant DNA was removed by digestion with RNase-free DNase (Qiagen). Complementary RNA was prepared from 2 μg of total RNA using 1-cycle target labeling and a control reagent kit (Affymetrix, Santa Clara, CA). Hybridization and signal detection of HG-U133 Plus 2.0 arrays (Affymetrix) were performed according to the manufacturer's instructions. The microarray datasets of (1) $Gdeg^{high}ROS^{low}$ and $Gdeg^{low}ROS^{high}$ HuH7 cells and (2) 253 tissue samples from HCC patients were normalized separately using the robust multiarray average method found in the R statistical software (v. 2.12.1) together with the Bioconductor package. Estimated gene-expression levels were obtained in log2-transformed values, and 62 control probe sets were removed for further analysis.

Gene Set Enrichment Analysis (GSEA). Biological functions associated with the malignant phenotype in HCC cells were investigated using GSEA v. 2.0.7 with MSigDB gene sets v. 3.0.[17] Probe sets marked as "present" by the Gene Expression Console software (Affymetrix) in at least one $Gdeg^{high}ROS^{low}$ or $Gdeg^{low}ROS^{high}$HuH7 cell were used for this analysis. Gene set category "C2 CP REACTOME," which is

based on the Reactome database (http://www.reactome.org), was used. For analysis of the gene expression profiles obtained from HCC patients, a custom gene set was employed using genes showing more than a 2-fold change between $Gdeg^{high}ROS^{low}$ and $Gdeg^{low}ROS^{high}$ HuH7 cells. Gene sets satisfying both criteria with $P < 0.05$ and a false discovery rate (FDR) <0.05 were considered significant.

Macrophage Migration Assay. To determine whether tumor cells induce macrophage/monocyte chemotaxis, the double chamber migration assay was performed using the RAW264 murine macrophage cell line (RIKEN Cell Resource Center, Tsukuba, Japan). Briefly, the migration of RAW264 cells was assayed using a transwell chamber (24-well plate, 8-μm pore; BD Biosciences, Bedford, MA). In the lower chamber, 7.5×10^4 tumor cells in 0.8 mL of media were seeded and incubated in serum-free media for 72 hours. RAW264 cells (5×10^4 in 0.3 mL serum free media) were then seeded into the upper chamber and incubated at 37°C for 4 hours. RAW264 cells found on the upper surface of the filter were removed using a cotton wool swab. Cells were then fixed with 100% methanol and stained using Giemsa solution and the number of cells migrating to the lower surface was counted. Each experiment was conducted in triplicate and the mean is shown.

Peritoneal Metastasis Model. Peritoneal metastatic potentials of cancer cells were assessed as reported.[18] Briefly, 10^5 $Gdeg^{high}ROS^{low}$ HCC cells or unsorted control cells were injected intraperitoneally into 5-week-old female NOD.CB17-$PRkdc^{Scid}$/J mice (n = 4 mice per group; Charles River Japan, Kanagawa, Japan). The care and use of animals was in accordance with institutional guidelines. The mice were monitored three times weekly for lethargy, weight loss, and abdominal enlargement. Mice were euthanized by cervical dislocation at 4 weeks and the number and weight of tumor nodules within the peritoneal cavity were counted.

Immunofluorescent Staining. Tissue sections were prepared according to standard procedures. After deparaffinization, slides were incubated in permeabilization buffer (0.2% Triton-PBS) for 30 minutes, followed by incubation in blocking buffer (3% bovine serum albumin [BSA]-PBS) for 1 hour and exposure to the primary antibodies (F4/80 1:200, BioLegend) overnight at 4°C. Sections were then treated for 30 minutes with the secondary antibody Alexa Fluor 568 tetramethylrhodamine isothiocyanate-conjugated anti-rat IgG (1:1,000, Sigma) and Hoechst 33342 solution for nuclear staining diluted in PBS and 3% BSA. After mounting the slides were visualized with a fluorescent microscope (Carl Zeiss, Germany).

Protein Network Analysis. To reveal functional relationships among genes differentially expressed in $Gdeg^{high}ROS^{low}$ HuH7 cells, the protein interaction network was analyzed. Genes up-regulated or down-regulated more than 1.1-fold between $Gdeg^{high}ROS^{low}$ and $Gdeg^{low}ROS^{high}$HuH7 cells were included in the network. Protein interaction data obtained from BIND (http://bond.unleashedinformatics.com), BioGRID (http://thebiogrid.org), and HPRD (http://www.hprd.org) were downloaded from the ftp site of the National Center for Biotechnology Information (NCBI; ftp://ftp.ncbi.nih.gov/gene/GeneRIF/interactions.gz). The protein interaction network was analyzed using Cytoscape software.[19]

Patients and Tissue Samples. In all, 187 patients underwent curative hepatectomy for HCC from 2004 to 2007 at Tokyo Medical and Dental University Hospital (Tokyo, Japan), and among these, 153 cases were randomly selected for this study. With Institutional Review Board approval, written informed consent was obtained from all patients (Permission No. 1080). Noncancerous liver tissue adjacent to HCC (n = 100) was snap-frozen in liquid nitrogen and stored at −80°C. Patients were followed up with assays for serum alpha-fetoprotein levels and protein induced by vitamin K absence or antagonists-II every month and with ultrasonography, computed tomography, and magnetic resonance imaging every 3 months. Median observation time was 9.86 months.

To divide patients into subgroups based on expression profiles of a particular gene set, gene-set enrichment patterns were analyzed using a method similar to that described by Ben-Porath et al.[20] For each patient, the number of genes that showed more than a 1.1-fold change in expression (either up-regulation or down-regulation) compared to the mean expression levels were counted. Patients who exhibited up-regulation of more than 30% of the genes in the gene set were classified as the high expression group. Likewise, patients who showed down-regulation of more than 30% of the genes in the gene set were classified as the low expression group. Samples that satisfied neither or both criteria above were classified as the moderate expression group. The recurrence-free survival rates among three groups were compared by Kaplan-Meier curves, followed by the log-rank test.

Statistical Analysis. Experimental data are expressed as mean values with 95% confidence intervals (CI) and were compared using a two-sided paired Student's t test. Statistical significance was defined as $P < 0.05$.

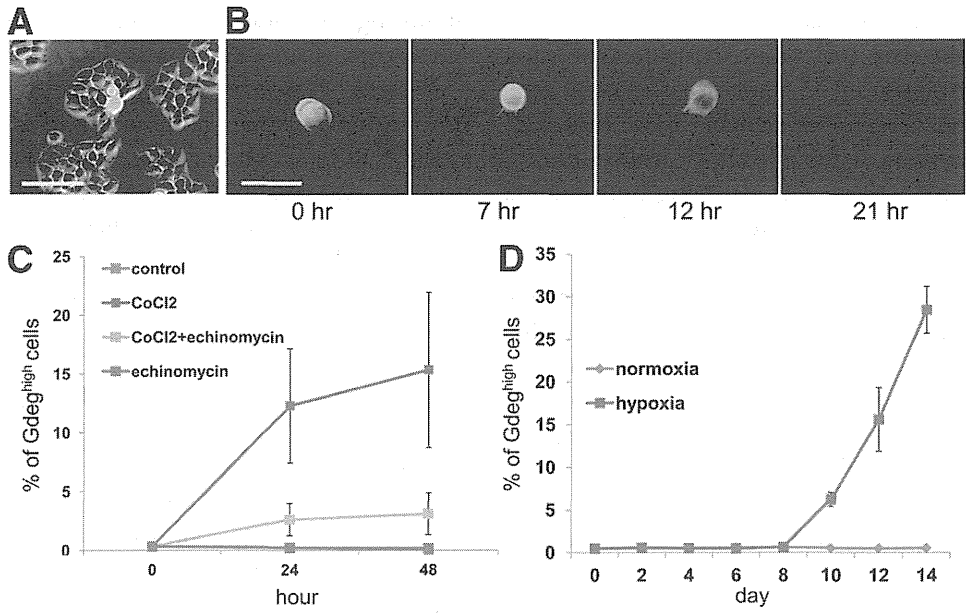

Fig. 1. (A) Frequency of cells with accumulation of Gdeg protein ($Gdeg^{high}$) in human HCC cultures (bar, 100 μm). (B) Asymmetric cell division of the $Gdeg^{high}$ HCC observed by time-lapse microscope. $Gdeg^{high}$ HCC cells asymmetrically divided into $Gdeg^{high}$ and $Gdeg^{low}$ HCC cells (bar, 50 μm). (C) The alteration of the $Gdeg^{high}$ proportion in the unsorted HCC cells after 24-hour and 48-hour treatment of $CoCl_2$ (100 μM) with or without echinomycin (10 nM); results are presented as means ± standard deviation from triplicate experiments. (D) The alteration of the $Gdeg^{high}$ proportion in the unsorted HCC cells under long-term hypoxic conditions (1% O_2); results are presented as means ± standard deviation from triplicate experiments.

Results

Characterization of CSC Proteasome Activity in Human HCC Cells. Human HCC cells were engineered to stably express ZsGreen-labeled degron (Gdeg) according to the previous report by Vlashi et al.[12] Cells displaying high levels of Gdeg ($Gdeg^{high}$) represented 0.5%-7.5% of the population in human HCC cell lines (Fig. 1A). In contrast, $Gdeg^{high}$ cells represented 0.1% of the population in human primary HCC (Supporting Fig. 1); however, only four generations were passaged without establishment. Isolation of the established $Gdeg^{high}$ cells and $Gdeg^{low}$ cells was performed using FACSAria II (BD Biosciences). As demonstrated by time-lapse microscopy, $Gdeg^{high}$ cells can asymmetrically divide into $Gdeg^{low}$ and $Gdeg^{high}$ cells, while $Gdeg^{low}$ cells never divide into $Gdeg^{high}$ cells. These results demonstrate some properties of CSCs and non-CSCs,[21] such as hierarchical division of CSCs and loss of stemness in differentiated non-CSCs (Fig. 1B; Supporting Video 1). In addition, the spheroid assay revealed that $Gdeg^{high}$ cells form slightly larger spheroids than unsorted cells (Supporting Fig. 2).

Effects of Hypoxia on HCC CSCs. Since pluripotent potentials in embryonic stem cells can be efficiently maintained under low oxygen levels[22] and hypoxia can contribute to CSC maintenance,[23] the effects of hypoxic conditions in unsorted HCC cells transfected with Gdeg were analyzed. The proportion of $Gdeg^{high}$ HCC cells significantly increased after 48-hour treatment with $CoCl_2$, an agent mimicking the activation of hypoxia-inducing factor (HIF).[24] The effects of $CoCl_2$ were blocked by echinomycin, a molecule inhibiting HIF-1 DNA binding activity (Fig. 1C) that has recently been reported to eradicate serially transplantable human acute myeloid leukemia (AML) in xenogeneic models by preferential elimination of CSCs.[25] The effects of long-term hypoxic treatment (1% O_2) were also analyzed in the unsorted HCC cells. $Gdeg^{high}$ cells represented 0.5% of the population on Day 1, but significantly increased to 28.0% on Day 14 (Fig. 1D). Similar to previous reports showing that CSCs are usually resistant to the conventional chemotherapy,[9] $Gdeg^{high}$ cells also demonstrated chemoresistance compared to unsorted cells under hypoxia conditions (Supporting Fig. 3). These results are consistent with reports showing that hypoxic conditions serve as a stimulus to reprogram cells towards normal stem cells and CSCs.[22,23]

CSCs Property of the HCC Subpopulation With Low Intracellular ROS Levels and Low Proteasome Activity. $Gdeg^{high}$ cells had a lower concentration of ROS than the unsorted cells based on the intracellular concentrations of MitoSOX Red staining. Intracellular ROS-positive cells (ROS^{high}) accounted for 71.0% ± 8.22% of the unsorted HuH7 HCC cells, but only

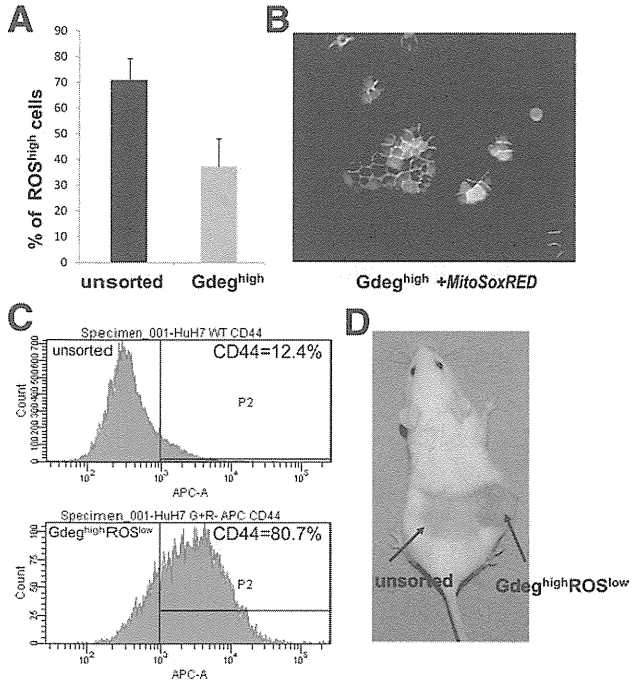

Fig. 2. (A) The proportion of ROS-positive cells (ROS^{high}) in unsorted HCC cells (left) and the sorted $Gdeg^{high}$ HCC cells (right) determined by FACS analysis with MitoSOX Red staining; results are presented as means ± standard deviation from triplicate experiments ($P < 0.05$). (B) $Gdeg^{high}$ and $Gdeg^{high}$ HCC cells stained with MitoSOX Red; (C) Flow cytometry histogram showing expression of CD44 positive cells in the $Gdeg^{high}ROS^{low}$ HuH7 cells (80.7%) and unsorted HuH7 cells (12.4%). (D) Tumorigenicity analysis using NOD/SCID mice; a tumor nodule was detected at the inoculation site of 10^2 $Gdeg^{high}ROS^{low}$ HCC cells, but not at the inoculation site of the unsorted cells.

37.2% ± 10.8% within the $Gdeg^{high}$ HuH7 cell population ($P < 0.05$). The $Gdeg^{high}$ group also contained a subpopulation of cells with low intracellular ROS levels ($Gdeg^{high}ROS^{low}$) (Fig. 2A).

To determine whether $Gdeg^{high}ROS^{low}$ HCC cells might possess certain stem cell-like properties, the expression of stem cell surface markers, CD133,[5] CD90,[6] EpCAM,[7] and CD44 was analyzed.[8] CD44-postiveness was detected in 80.7% of $Gdeg^{high}ROS^{low}$ HuH7 cells, but in only 12.4% of unsorted HuH7 cells (Fig. 2C). EpCAM and CD90 expression were increased in the $Gdeg^{high}ROS^{low}$ HLF cells compared to the unsorted HLF cells (EpCAM; 6.0% versus 2.7%, CD90; 55.9% versus 44.6%).

An important test for validating whether cells are CSCs is the identification of a cancer initiation population demonstrated by increased tumorigenicity *in vivo*. Different cell numbers from each population were injected subcutaneously into nonobese diabetic / severe combined immunodeficient (NOD/SCID) mice in numbers ranging from 10^2 to 10^5 cells per injection. $Gdeg^{high}ROS^{low}$ HCC cells had higher tumorigenic capacity than unsorted cells. As few as 10^2 $Gdeg^{high}ROS^{low}$ HCC cells could form a subcutaneous tumor (Fig. 2D, Table 1; Supporting Table 2). Cancer initiation frequency was calculated using L-Calc Software[26] (Stem Cell Technologies), and significance was determined by chi-square analysis using ELDA (Walter and Eliza Hall Bioinformatics).[26] The cancer initiation frequency was 1 in 2,083 (95% CI = 739 to 5,867) for $Gdeg^{high}ROS^{low}$ HCC cells and 1 in 79,189 (95% CI = 31,651 to 198,128) for unsorted cells ($P < 0.001$). These data validate that CSCs are significantly enriched in the $Gdeg^{high}ROS^{low}$ subpopulation compared to unsorted HCC cells.

Tumor-Host Interactions of HCC CSCs. Comprehensive gene expression analysis in $Gdeg^{high}ROS^{low}$ HCC cells was performed to acquire the CSC gene profile. As described in a previous report,[13] GSEA based on the Reactome database[27] was utilized to determine the biological pathways activated or inactivated in $Gdeg^{high}ROS^{low}$ HCC cells. The GSEA demonstrated significant enrichment in 8 gene sets (Supporting Table 3), and the gene set "chemokine_receptors_bind_chemokines" showed the lowest FDR (Fig. 3A). A protein interaction network was then constructed using 12,890 probe sets with at least 10% change in expression levels. To more closely investigate molecular networks associated with chemokines, a subnetwork of 2-hop neighbors from chemokine ligands and receptors including CXCL, CCL, CX3CL, XCL, CXCR, CCR, CX3CR, and XCR family genes was generated (Fig. 3B).

The ability of $Gdeg^{high}ROS^{low}$ HCC cells to induce macrophage chemotaxis was determined using a chemotaxis assay and the RAW264 murine macrophage-like cell line (Fig. 3C). $Gdeg^{high}ROS^{low}$ HCC cells significantly facilitated RAW264 cell migration compared to their counterparts and unsorted controls (average number of cells that migrated to the lower chamber, $Gdeg^{high}ROS^{low}$ HCC cells versus unsorted HCC cells: difference = 192, 95% CI = 61 to 323, $P = 0.0153$, n = 3; $Gdeg^{high}ROS^{low}$ HCC cells versus $Gdeg^{low}ROS^{high}$ HCC cells: difference = 196, 95%

Table 1. Enhanced Tumor Formation by $Gdeg^{high}ROS^{low}$ HCC Cells

Number of Cells Injected	Fraction (%) of Injected Mice That Developed Tumors	
	Injected With $Gdeg^{high}ROS^{low}$ Cells	Injected With Unsorted Cells
10^2	3/6 (50%)	0/6 (0%)
10^3	4/6 (66.7%)	1/6 (16.7%)
10^4	5/6 (83.3%)	2/6 (33.3%)
10^5	5/6 (83.3%)	3/6 (50%)

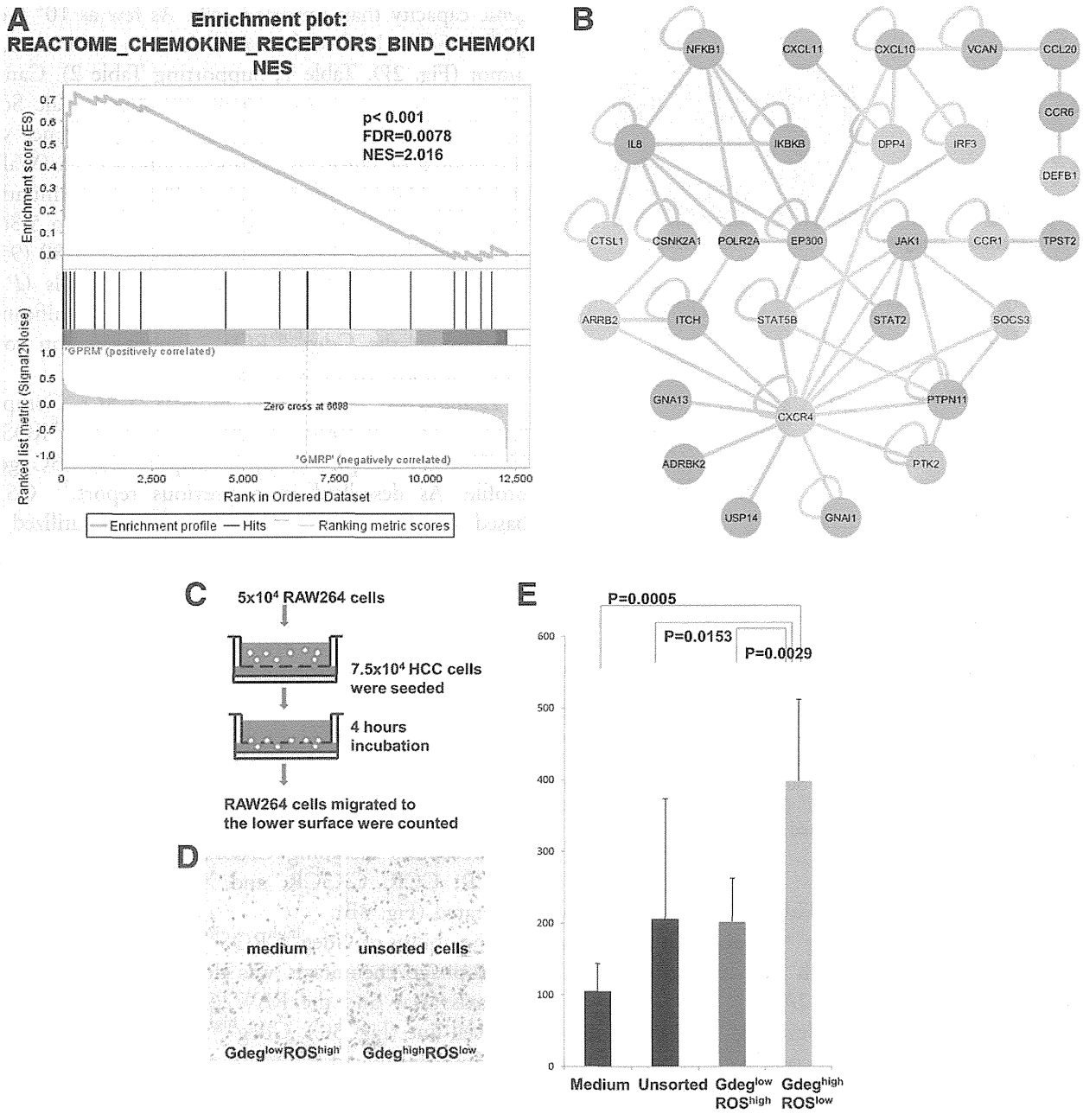

Fig. 3. (A) GSEA evaluation of gene-expression profile associated with Gdeg^{high}ROS^{low} HCC cells; the gene set "chemokine_receptors_bind_-chemokines" showed the lowest FDR ($P < 0.001$; FDR = 0.0078; NES = 2.016). (B) A protein interaction network constructed using 12,890 probe sets with at least 10% change in expression levels; a sub-network of 2-hop neighbors from chemokine ligands and receptors was extracted. (C) Diagram of the double chamber migration assay using a RAW264 murine macrophage-like cell line. (D) Giemsa staining for the RAW264 cells migrating to the lower surface. (E)The number of the RAW264 cells migrated to the lower surface induced by Gdeg^{high}ROS^{low} HCC cells compared to Gdeg^{low}ROS^{high} HCC cells, unsorted HCC cells, and medium. Each experiment was conducted in triplicate, and data are presented as the means ± 95% CI.

CI = 112 to 280, $P = 0.0029$, n = 3, Gdeg^{high}ROS^{low} HCC cells versus medium: difference = 292, 95% CI = 214 to 370, $P < 0.001$, n = 3) (Fig. 3D,E). Facilitated migration of host macrophages may be associated with niche formation of the HCC CSCs subpopulation.

To investigate whether the HCC cells established *in vivo* metastasis, Gdeg^{high}ROS^{low} or unsorted HCC cells were administered intraperitoneally in a NOD/SCID mouse model, as described previously.[18] Peritoneal metastases were assessed by counting the number of nodules and evaluating tumor weight in the mesentery and peritoneal walls. The tumor weight (average weight of dissemination nodules: Gdeg^{high}ROS^{low} HCC cells versus unsorted HCC cells, difference = 0.197, 95% CI = −0.304 to 0.699, $P = 0.3728$,